NTNU

Norwegian University of
Science and Technology

Do the LHAASO Galactic diffuse emission data require a contribution from unresolved sources?

Presented by: Vittoria Vecchiotti

Based on work done in collaboration with: G. Peron, E. Amato, G. Morlino, S. Menchiari, F. L. Villante and G. Pagliaroli

TeV Particle Astrophysics, 26-30 August 2024, Chicago

Outline:

1. Galactic gamma-ray diffuse emission model;

2. Source model, compatibility with LHAASO KM2A measurements, unresolved source contribution;

   Cataldo et al. Astrophys.J. 904 (2020)

3. Comparisons with LHAASO diffuse emission measurements.

   Vecchiotti et al (2024), in preparation

LHAASO diffuse emission measurements:

$\varphi_{\gamma,\mathrm{diff}}^{LHAASO}$ → The LHAASO collaboration provided a measurement of the Galactic diffuse γ-ray emission in the energy range 10 TeV to 1 PeV in two sky regions by masking the contribution of known sources. *Z. Cao et al. 2023, Phys. Rev. Lett,131*

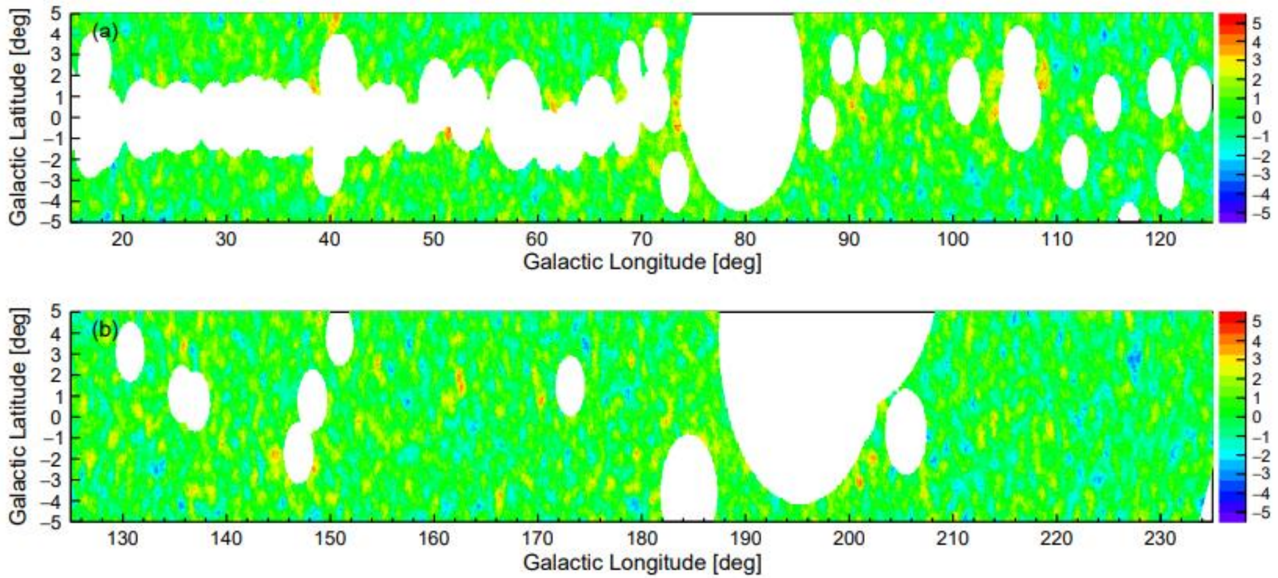

Do the LHAASO Galactic diffuse emission data are contaminated unresolved sources?

$$\varphi_{\gamma,\mathrm{diff}}^{LHAASO} = \varphi_{\gamma,S}^{UnRes} + \varphi_{\gamma,\mathrm{diff}}$$

Population study H.E.S.S.

Models:
Assumptions on the CR spatial and energy distributions, cross-section, and ISM.

Diffuse gamma-ray emission:

1. Differential inelastic cross section of pp interaction.

2. Interstellar gas distribution in the Galaxy

$$\varphi_\gamma(E_\gamma, \hat{n}_\gamma) = \int_{E_\gamma}^{\infty} dE \, \frac{d\sigma(E, E_\gamma)}{dE_\gamma} \int_0^{\infty} dl \, \varphi_{CR}(E, \bar{r}_\odot + l\hat{n}_\gamma) n_H \, (\bar{r}_\odot + l\hat{n}_\gamma)$$

3. Cosmic-ray energy and spatial distribution

1. Cross section:

$$f(E_\gamma) = \int_{E_\gamma}^{\infty} dE \frac{d\sigma(E, E_\gamma)}{dE_\gamma} \varphi_{CR}(E)$$

We compare:

- different parameterization based on different MC codes SIBYLL, QGSJET, Pythia8, and Geant4 (*Kafexhiu et al 2014*);
- SIBYLL (*Kelner et al 2006*);
- AAFRAG based on QGSJET-II-04m (*M. Kachelriess et al 2022*)

1. Cross section:

$$f(E_\gamma) = \int_{E_\gamma}^{\infty} dE \frac{d\sigma(E, E_\gamma)}{dE_\gamma} \varphi_{CR}(E)$$

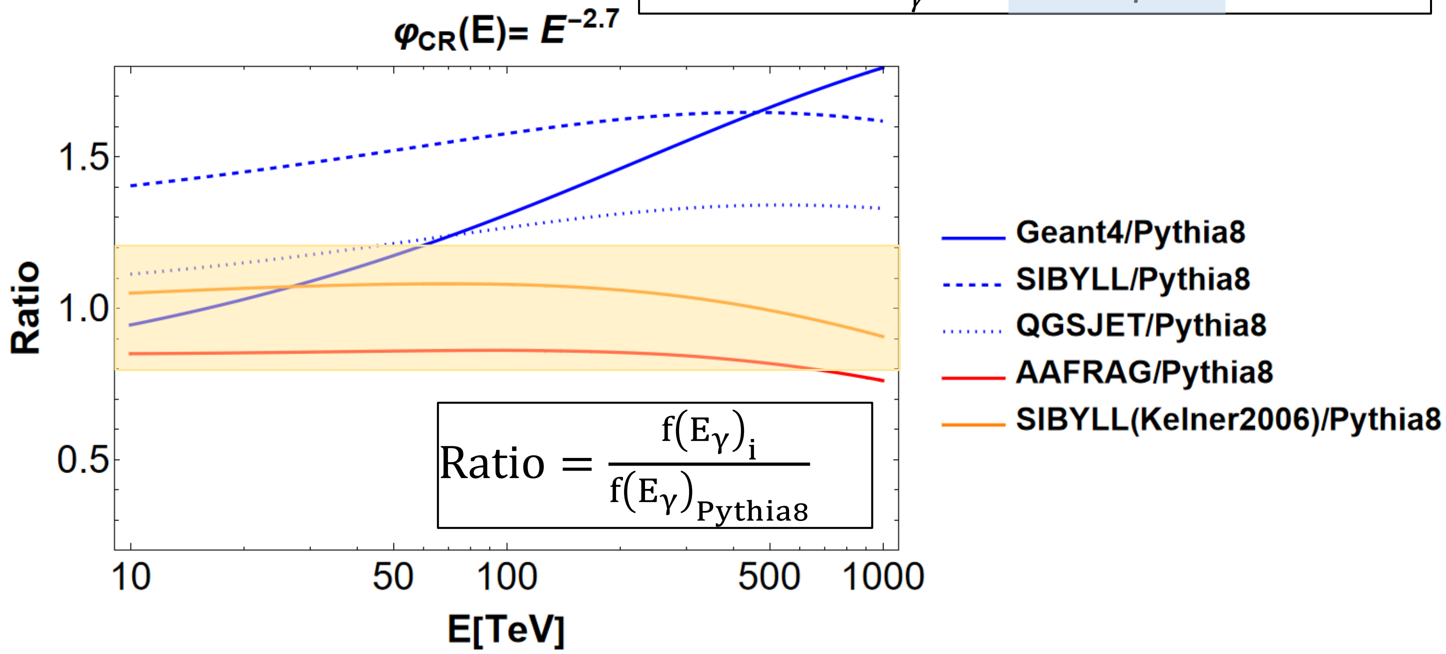

We compare:

- different parameterization based on different MC codes SIBYLL, QGSJET, Pythia8, and Geant4 (*Kafexhiu et al 2014*);
- SIBYLL (*Kelner et al 2006*);
- AAFRAG based on QGSJET-II-04m (*M. Kachelriess et al 2022*)

1. Cross section:

$$f(E_\gamma) = \int_{E_\gamma}^{\infty} dE \frac{d\sigma(E, E_\gamma)}{dE_\gamma} \varphi_{CR}(E)$$

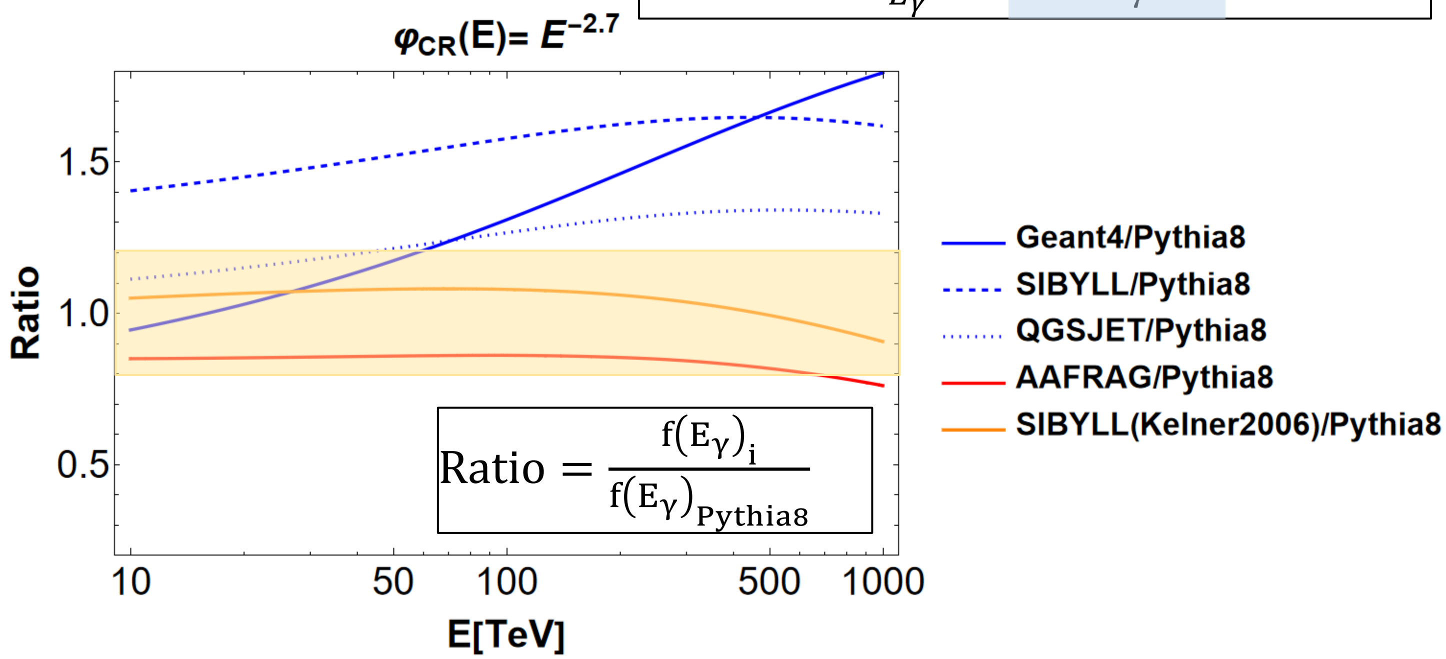

We compare:

- different parameterization based on different MC codes SIBYLL, QGSJET, Pythia8, and Geant4 (*Kafexhiu et al 2014*);
- SIBYLL (*Kelner et al 2006*);
- AAFRAG based on QGSJET-II-04m (*M. Kachelriess et al 2022*)

Assumptions cross section:

We take AAFRAG for the fiducial case and SIBYLL (*Kafexhiu et al 2014*) to include uncertainties.

1. Cross section:

$$f(E_\gamma) = \int_{E_\gamma}^{\infty} dE \frac{d\sigma(E, E_\gamma)}{dE_\gamma} \varphi_{CR}(E)$$

$\varphi_{CR}(E) = E^{-2.7}$

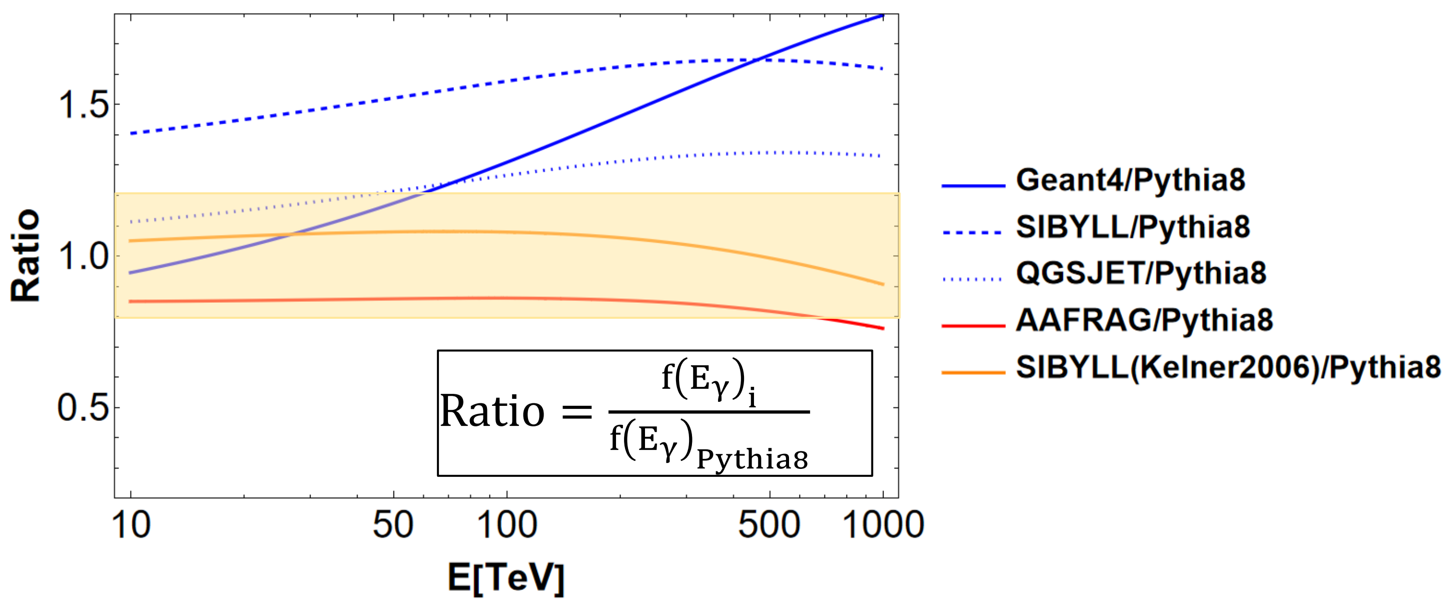

We compare:

- different parameterization based on different MC codes SIBYLL, QGSJET, Pythia8, and Geant4 (*Kafexhiu et al 2014*);
- SIBYLL (*Kelner et al 2006*);
- AAFRAG based on QGSJET-II-04m (*M. Kachelriess et al 2022*)

Assumptions cross section:

We take AAFRAG for the fiducial case and SIBYLL (*Kafexhiu et al 2014*) to include uncertainties.

2. ISM:

$$n_c = \frac{\int_{\Delta\Omega} d\Omega \int_0^\infty dl \, n_H(\bar{r}_{Sun} + l\hat{n}_\gamma)}{\Delta\Omega}$$

- Dust (masked): *PLANCK (Aghanim et al. 2016)*
  $n_{c,inner} = 7.85068 \times 10^{21}\ cm^{-2}$
  $n_{c,outer} = 5.84937 \times 10^{21}\ cm^{-2}$
- Galprop (masked):
  $n_{c,inner} = 9.47769 \times 10^{21}\ cm^{-2}$
  $n_{c,outer} = 8.72069 \times 10^{21}\ cm^{-2}$

Galprop provides $\sim 20\%$ more target than the dust in the inner region and $\sim 50\ \%$ in the outer region

Assumptions ISM:

We take Galprop for the fiducial case and the Dust to include uncertainties.

3. Cosmic ray distribution: $\varphi_{CR}(E,\vec{r}) = \varphi_{CR,Sun}(E\ )g\ (\vec{r},R)\ h(E,\vec{r})$

3. Cosmic ray distribution:

$$\varphi_{CR}(E,\vec{r}) = \varphi_{CR,Sun}(E\ )g\ (\vec{r},R)\ h(E,\vec{r})$$

★ Assumption CR spectrum:

We take the data-driven CR spectrum from ***Dembinski et al 2018*** for the fiducial case and **Protons (KASKADE)** + ***Dembinski et al 2018*** to include uncertainties.

Protons

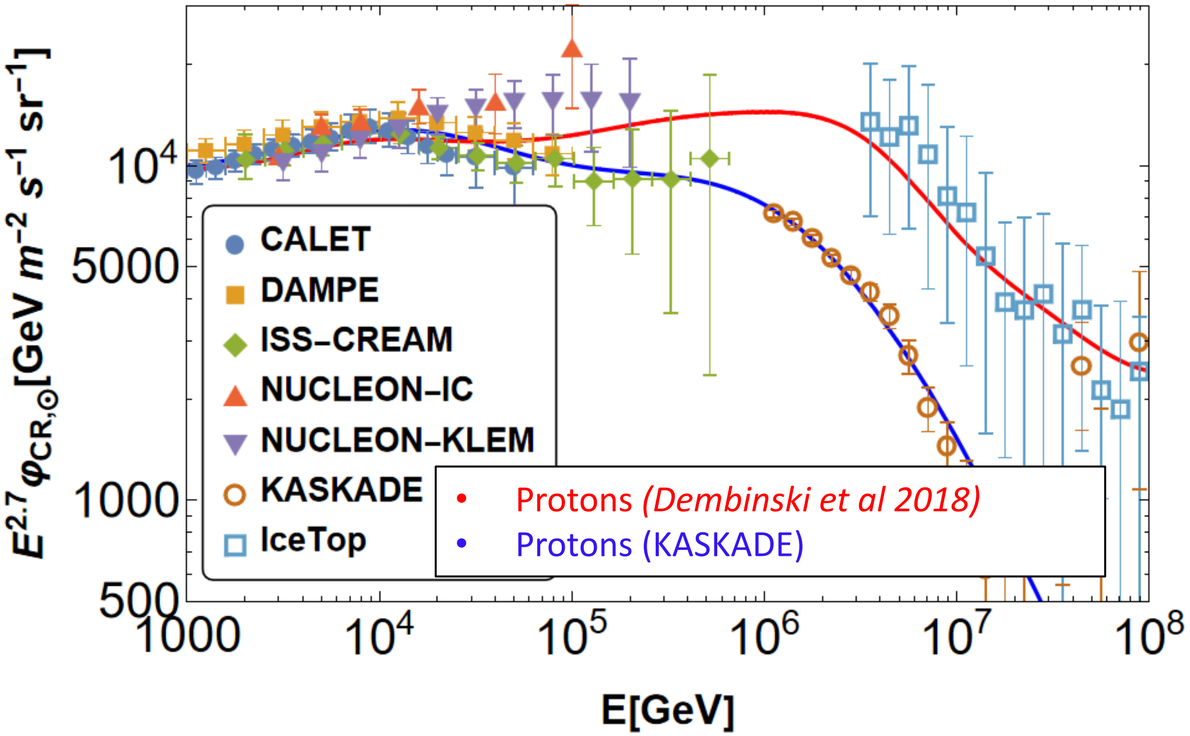

All Particle Spectrum

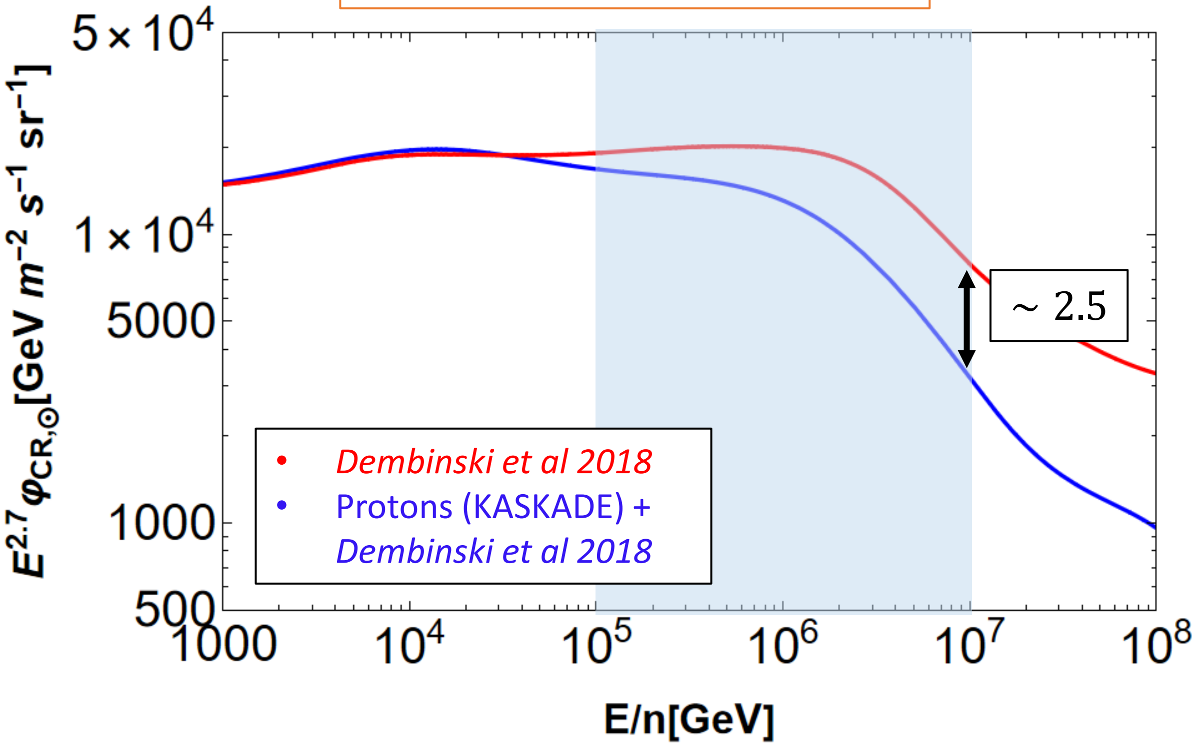

3. Cosmic ray distribution: $\varphi_{CR}(E,\vec{r}) = \varphi_{CR,Sun}(E)\, g(\vec{r},R)\, h(E,\vec{r})$

★ Assumption CR spectrum: We take the data-driven CR spectrum from ***Dembinski et al 2018*** for the fiducial case and **Protons (KASKADE)** + ***Dembinski et al 2018*** to include uncertainties.

★ g(r) is determined by the distribution of the CR sources $f_s(\vec{r})$ (proportional to the SNR number density by Green et al. (2015), and by the propagation of CR in the Galactic magnetic field.

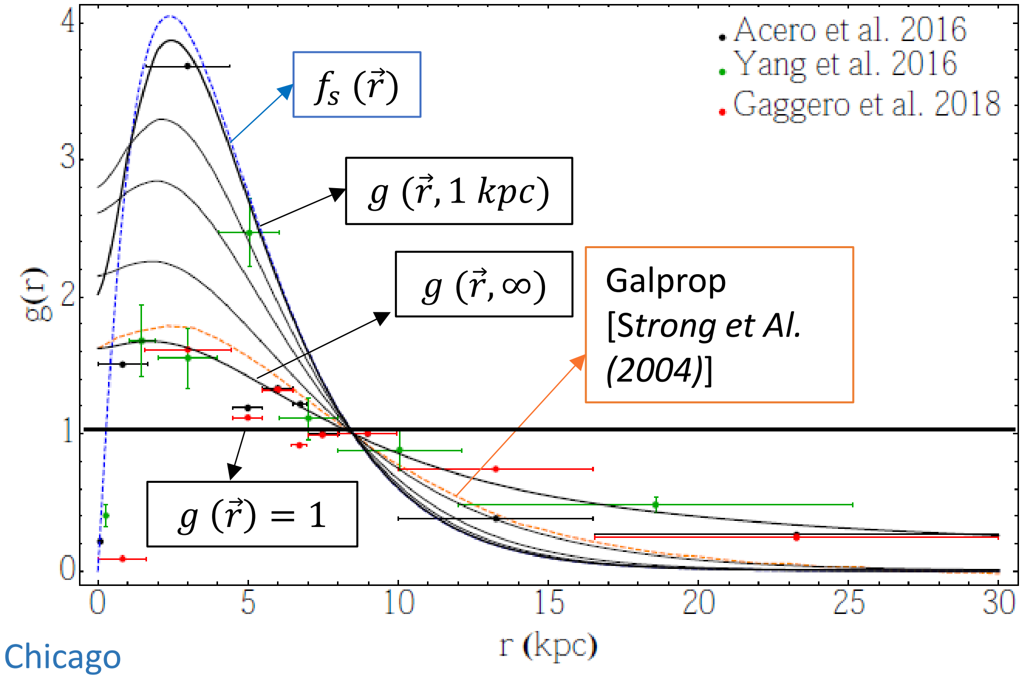

3. Cosmic ray distribution: $\varphi_{CR}(E,\vec{r}) = \varphi_{CR,Sun}(E)\,g(\vec{r},R)\,h(E,\vec{r})$

★ Assumption CR spectrum: We take the data-driven CR spectrum from ***Dembinski et al 2018*** for the fiducial case and **Protons (KASKADE)** + ***Dembinski et al 2018*** to include uncertainties.

★ g(r) is determined by the distribution of the CR sources $f_s(\vec{r})$ (proportional to the SNR number density by Green et al. (2015), and by the propagation of CR in the Galactic magnetic field.

★ **2 cases: with and without spatially dependent CR spectral index**
(from the analysis of the FermiLAT data at $\sim 20\ GeV$
Acero et al. (2016), Yang et al. (2016), Gaggero et al. (2018)

$$h(E,\vec{r}) = \left(\frac{E}{20\ GeV}\right)^{\Delta(\vec{r})}$$

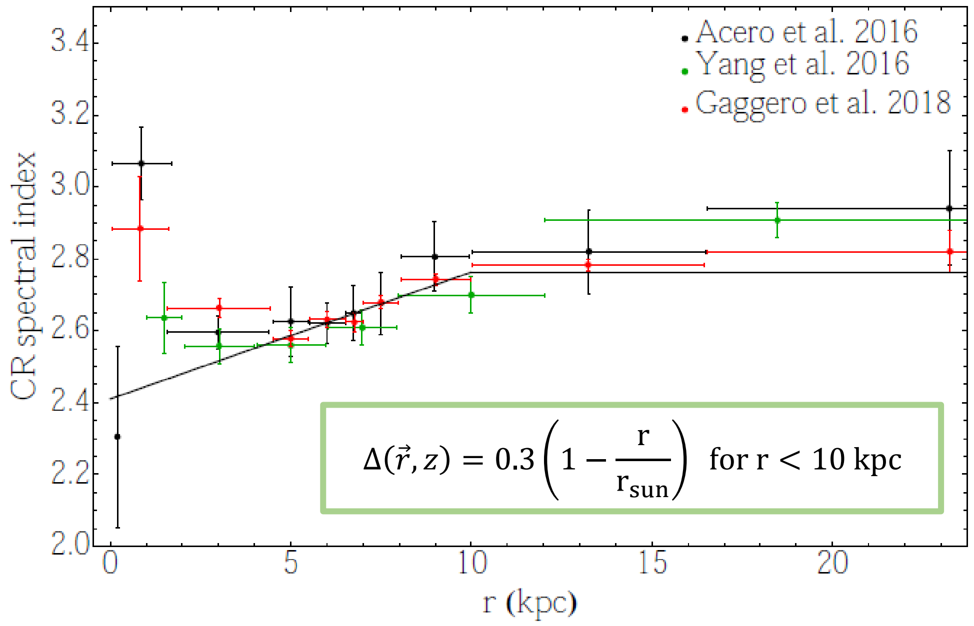

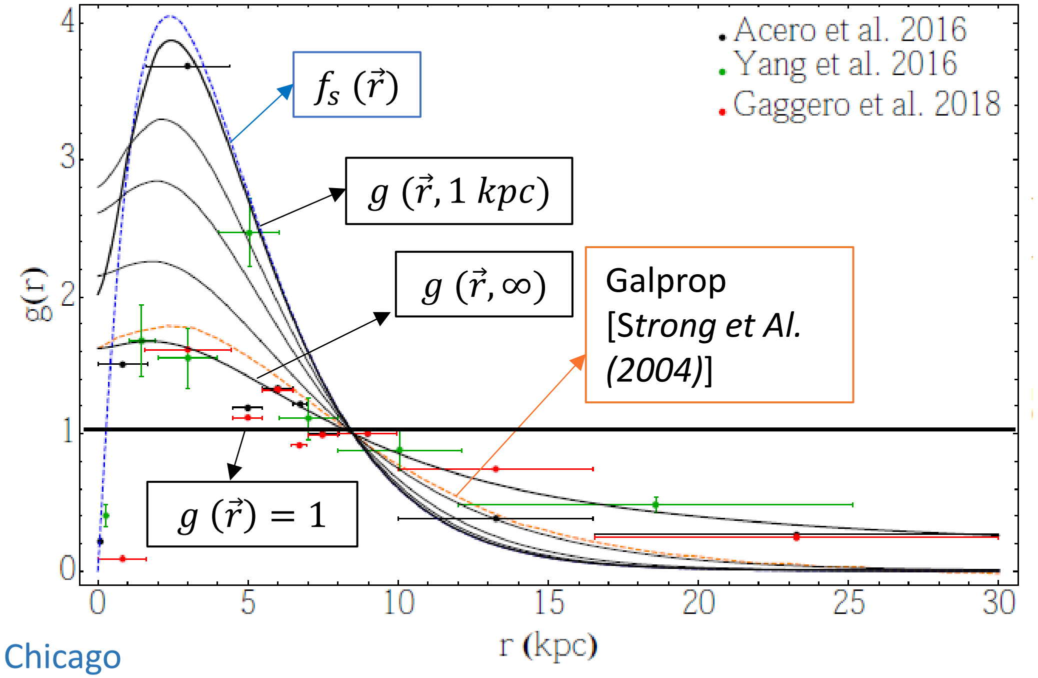

Comparison with LHAASO (standard diffusion):

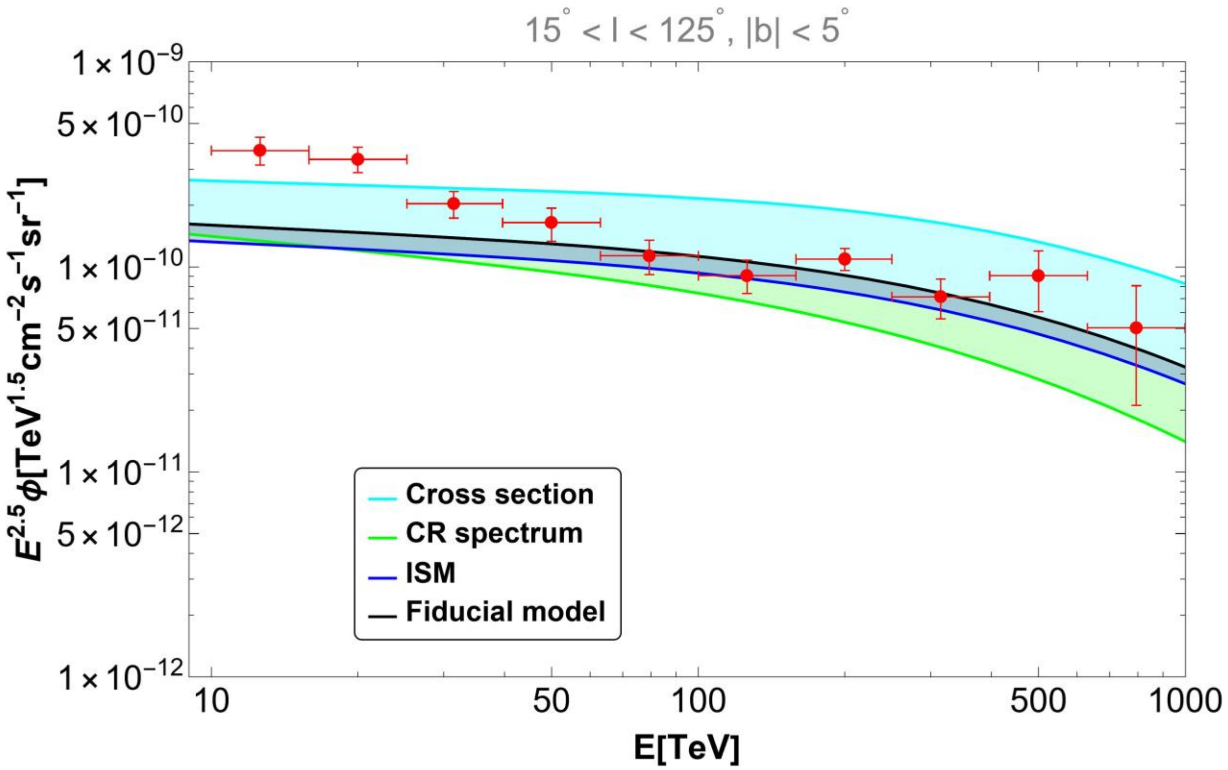

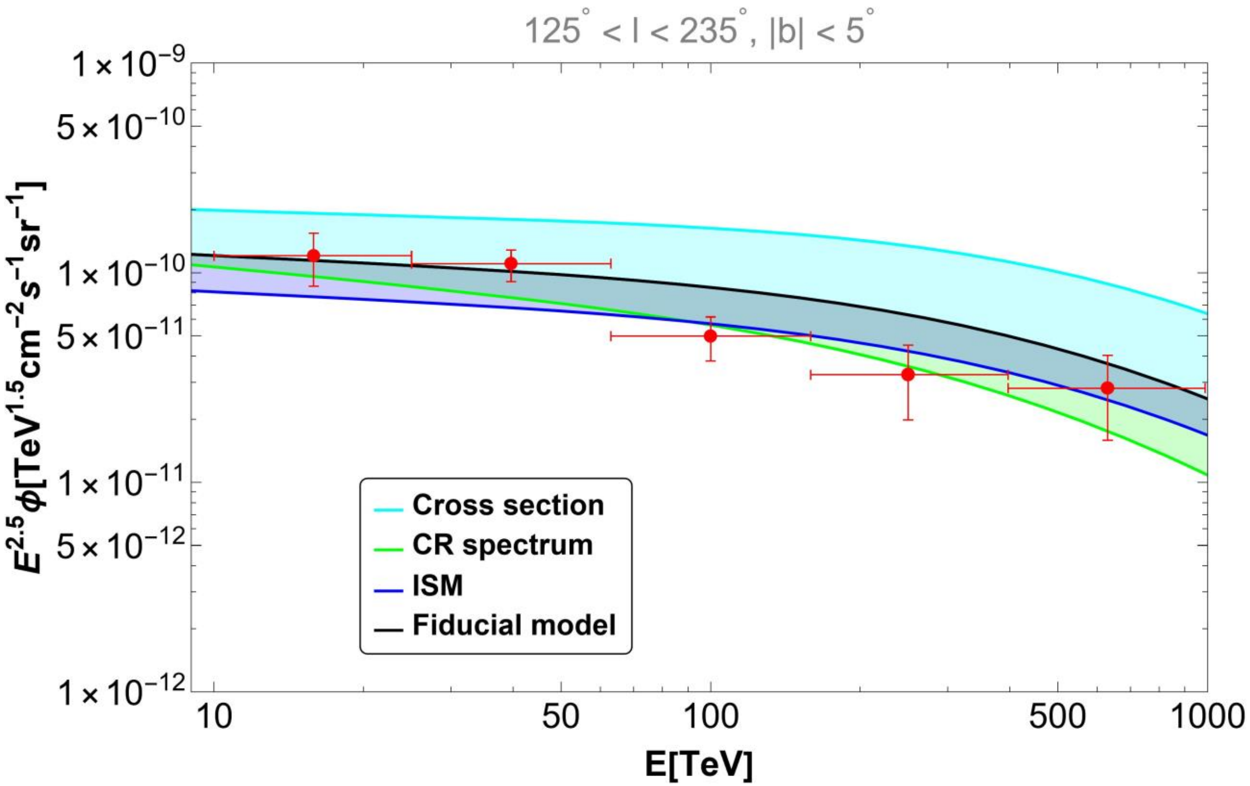

- LHAASO data can be explained by the ''truly'' diffuse emission in the outer region and in the inner region above ~ 30 TeV;

The contribution from unresolved sources must be negligible.

Pulsar Wind Nebulae population:

Cataldo et al. *Astrophys.J.* 904 (2020); Pagliaroli et al, *Universe*, 9,881 (2023)

We built a synthetic population of PWNe using the best fit of the maximum luminosity in the energy range $1 - 100$ TeV: $L_{max} = 2.2 \times 10^{35}$ erg/s and the spin-down down timescale: $\tau_{sd} = 2.9$ kyrs derived from fitting the brightest sources of the HGPS.

Assumptions:

- Latitude, longitude, and radius are extracted from the Lorimer distribution that scales as $\exp(-|z|/H)$ with $H = 0.05$ kpc (it is the value that provides the best chi-square in the fit of HGPS data);
- The age of sources t_{age} is extracted uniformly in the interval [1,10^6] yr;
- The luminosity is calculated from: $L = L_{max}\left(1 + \frac{t_{age}}{\tau_{sd}}\right)^{-2}$
- Spectrum: power-law with exponential cut-off ($\mathrm{E_{cut}} = 100$ TeV), spectral index fixed to: 2.4.

Source contributions:

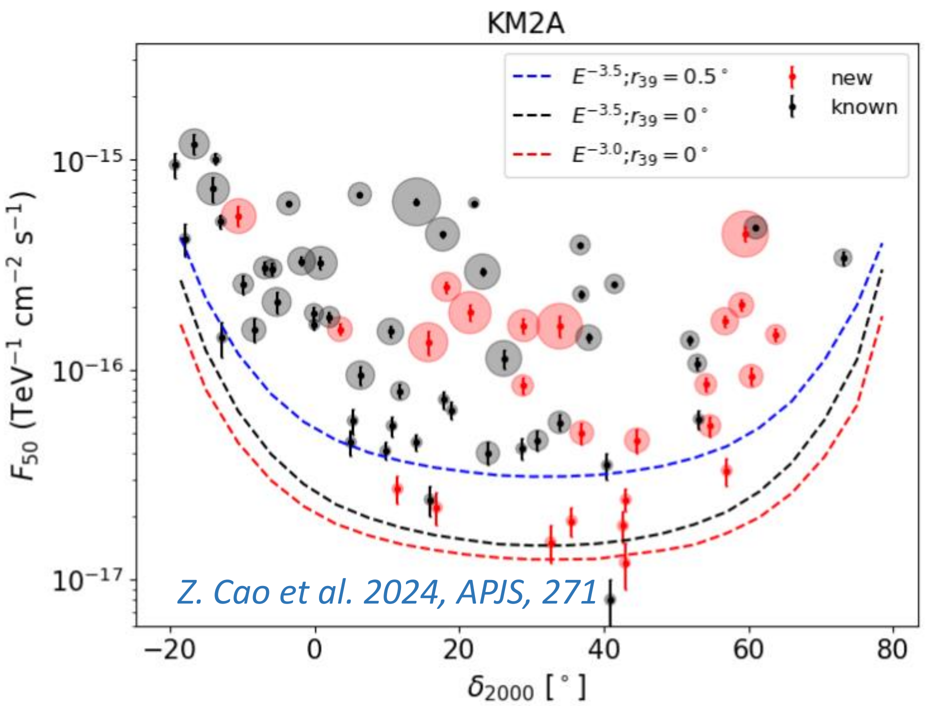

"The flux sensitivity is defined as the flux normalization required to have 50% probability of detecting a source at 5σ level"

At 50 TeV the differential threshold of point-like sources depends only mildly on the spectral assumption.

Def: Resolved sources: $\phi_{50} > \phi_{th,50}$, $\varphi[TeV^{-1}\ cm^{-2}s^{-1}]$

		N_R	φ_R	φ_{UNR}	$\varphi_{UNR,H}$
$15^\circ < l < 235^\circ$	MC	84^{+7}_{-5}	$1.69^{+0.62}_{-0.43} \times 10^{-14}$	$2.82^{+0.15}_{-0.14} \times 10^{-15}$	–
	KM2A	76	1.72×10^{-14}	–	–
$15^\circ < l < 125^\circ$	MC	73^{+5}_{-8}	$1.32^{+0.37}_{-0.33} \times 10^{-14}$	$2.56^{+0.14}_{-0.16} \times 10^{-15}$	$2.23^{+0.34}_{-0.36} \times 10^{-16}$
	KM2A	59	1.44×10^{-14}	–	–
$125^\circ < l < 235^\circ$	MC	12^{+3}_{-2}	$2.82^{+1.8}_{-1.1} \times 10^{-15}$	$2.53^{+0.46}_{-0.35} \times 10^{-16}$	$2.08^{+0.49}_{-0.34} \times 10^{-16}$
	KM2A	16	2.74×10^{-15}	–	–

Results:

- The predicted number and flux of resolved sources are compatible with the KM2A quantities within 2σ;
- The unresolved source flux is suppressed by 91 % and 18 % in the inner and outer regions, respectively.

Comparison with LHAASO (standard diffusion):

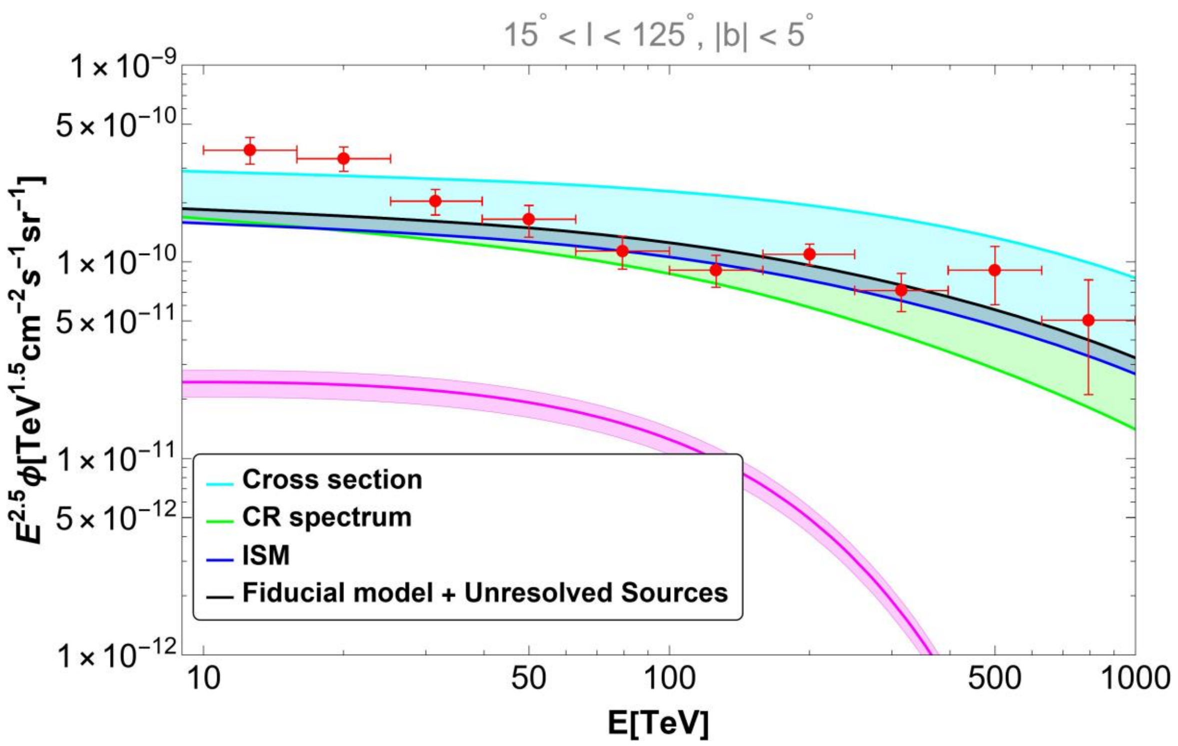

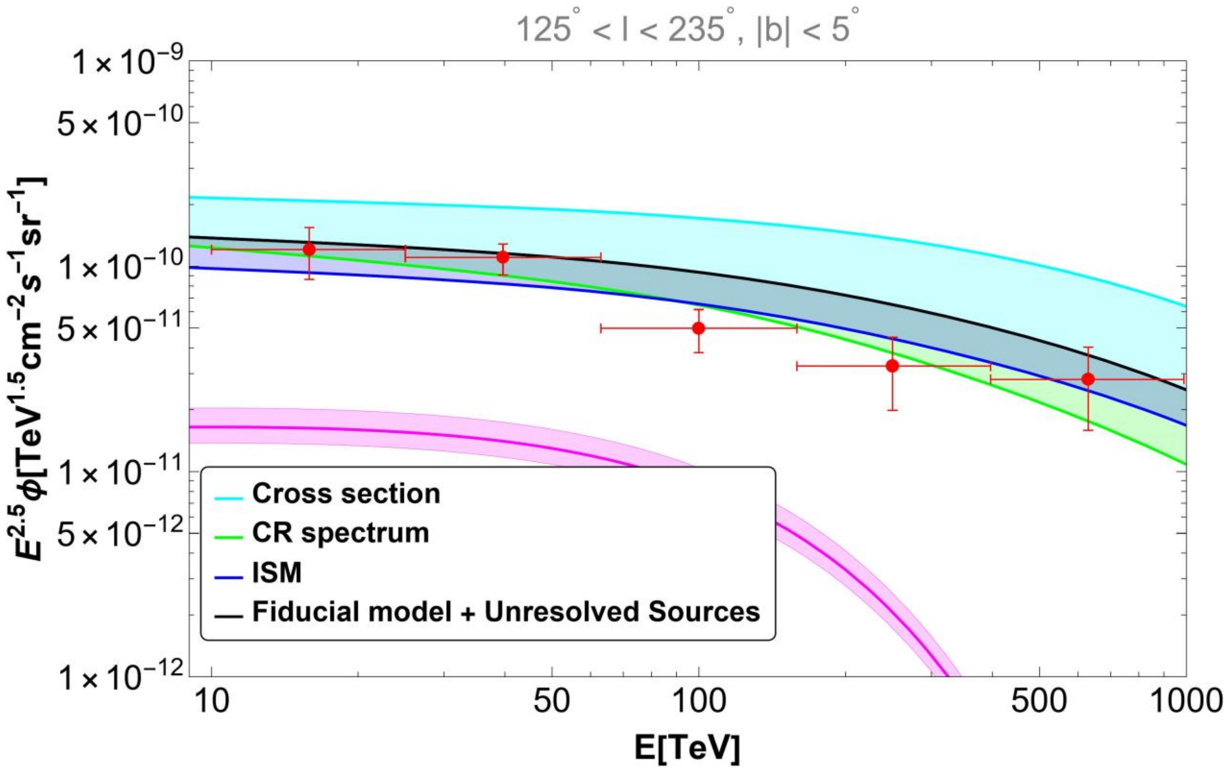

- The masks cancel out most of the unresolved source contributions. Unresolved sources contribute $\sim 15\%$ of the fiducial model at 50 TeV in both regions;

Effect of LHAASO masks on the hardening:

Def: hardening= spatially dependent CR spectral index

$\mathit{Inner\ Region}: 15° < l < 125°$

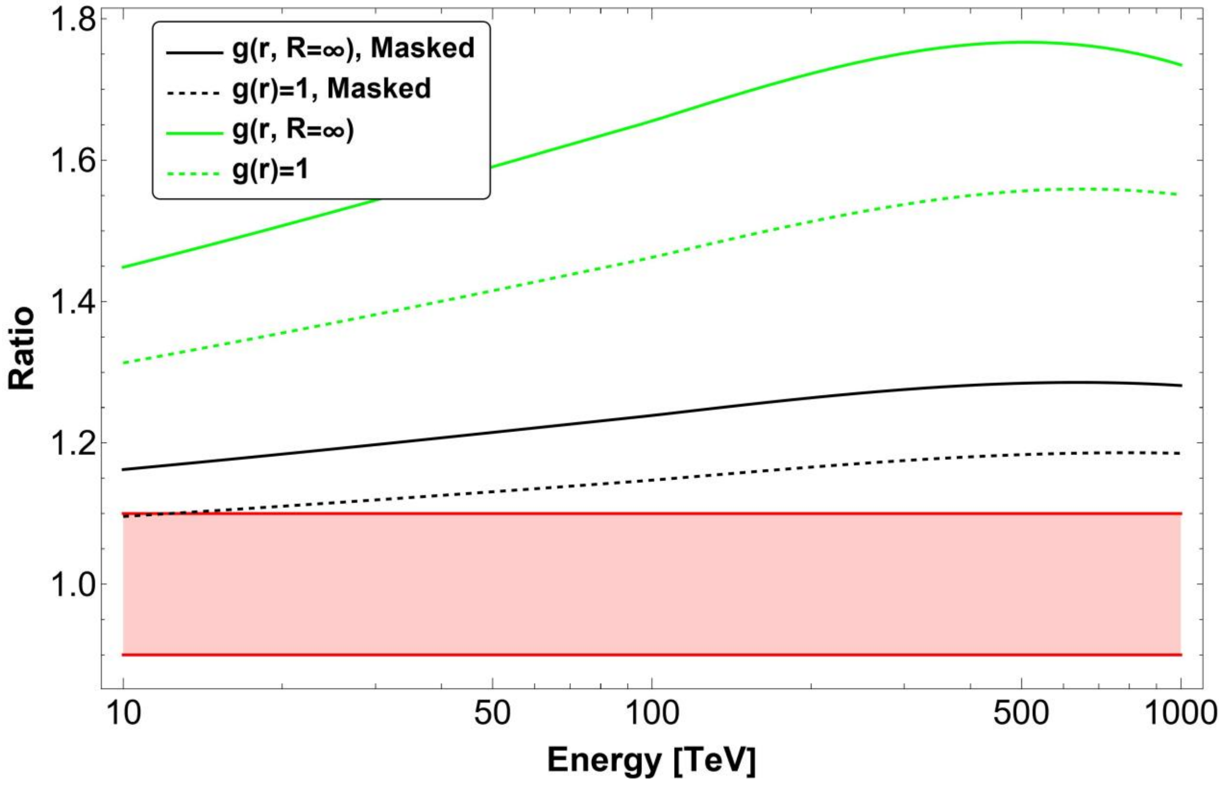

$$\textbf{Ratio} = \frac{\varphi_{\textbf{hardening}}}{\varphi_{\textbf{standard}}}$$

The ratio is ***independent*** of the cross-section, ISM and CR spectrum but it ***depends*** on the CR spatial distribution

Effect of LHAASO masks on the hardening:

Def: hardening= spatially dependent CR spectral index

$Inner\ Region: 15° < l < 125°$

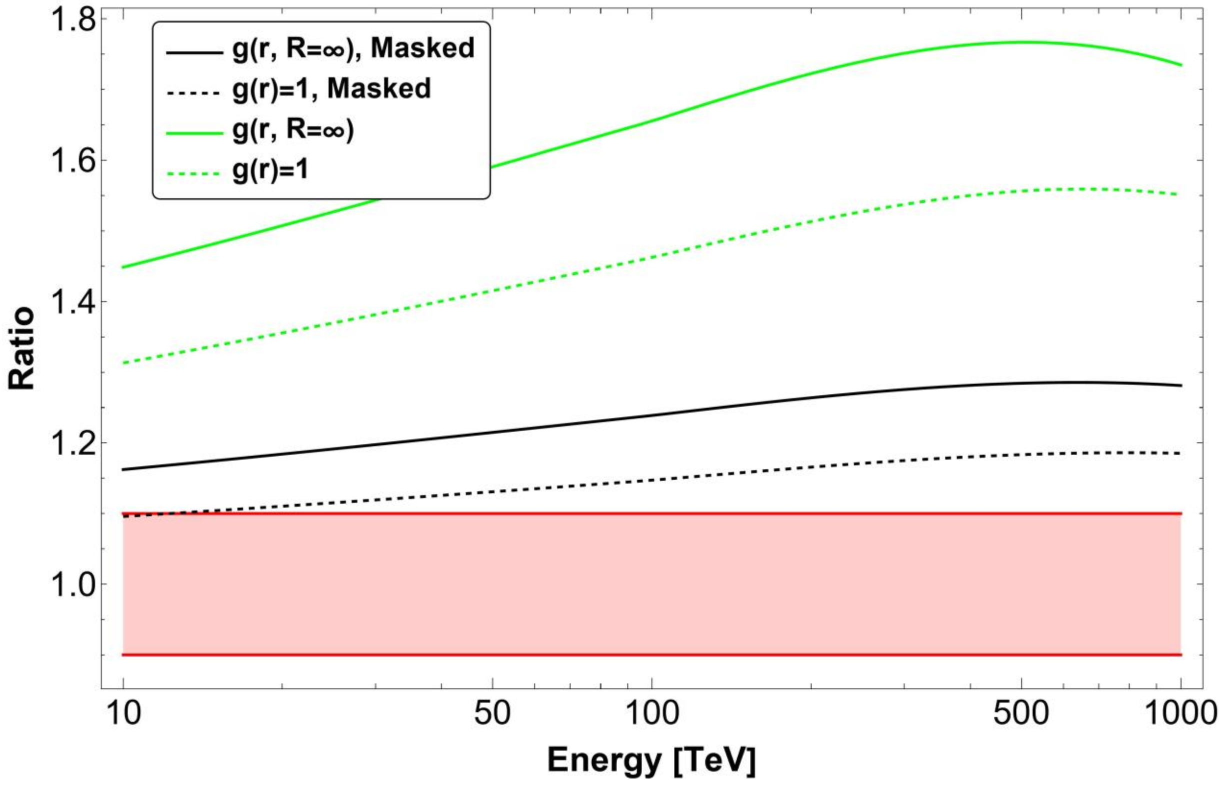

$$\mathbf{Ratio} = \frac{\boldsymbol{\varphi}_{\mathbf{hardening}}}{\boldsymbol{\varphi}_{\mathbf{standard}}}$$

The ratio is ***independent*** of the cross-section, ISM and CR spectrum but it ***depends*** on the CR spatial distribution

- $g(r, R = \infty)$: The $\boldsymbol{\varphi}_{\mathbf{hardening}}$ produces 76 % more signal than $\boldsymbol{\varphi}_{\mathbf{standard}}$ at 500 TeV ;
- $g(r) = 1$: The $\boldsymbol{\varphi}_{\mathbf{hardening}}$ produces 55% more signal than $\boldsymbol{\varphi}_{\mathbf{standard}}$ at 500 TeV

Effect of LHAASO masks on the hardening:

Def: hardening= spatially dependent CR spectral index

$Inner\ Region: 15° < l < 125°$

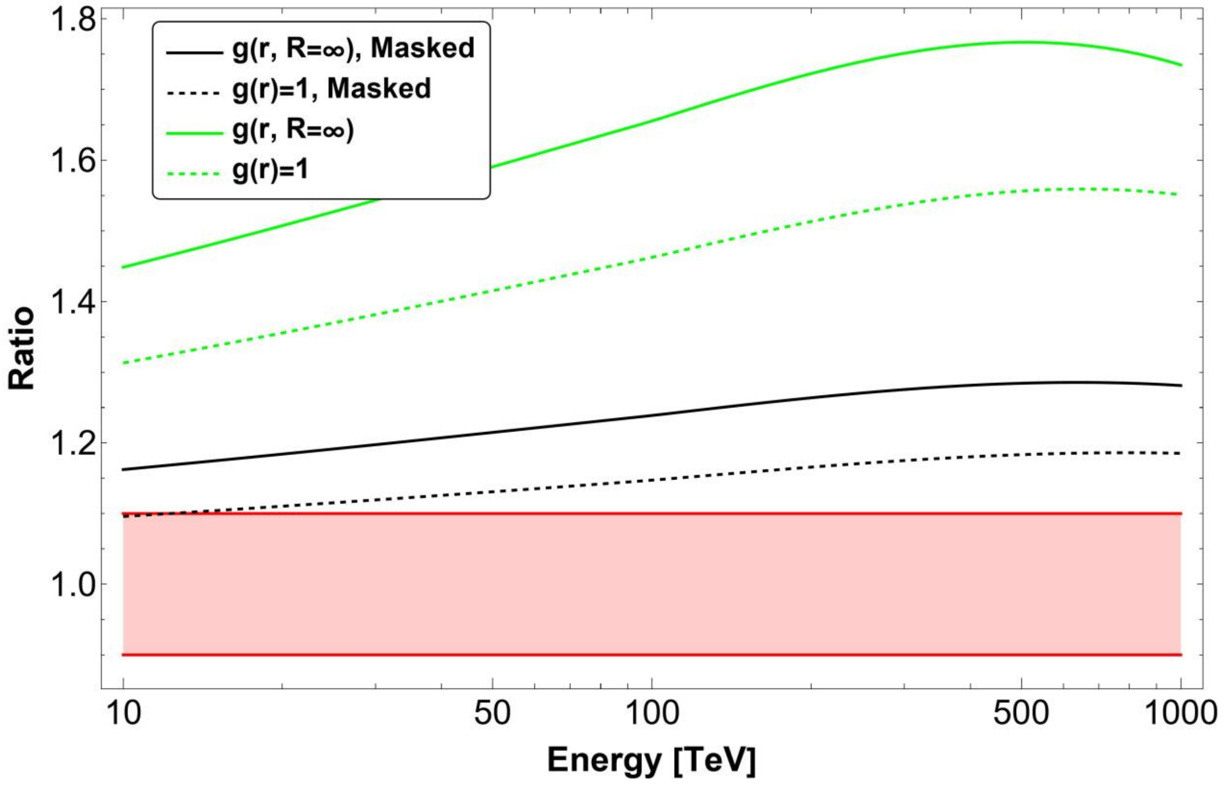

$$\textbf{Ratio} = \frac{\boldsymbol{\varphi}_{\textbf{hardening}}}{\boldsymbol{\varphi}_{\textbf{standard}}}$$

The ratio is ***independent*** of the cross-section, ISM and CR spectrum but it ***depends*** on the CR spatial distribution

- $g(r, R = \infty)$: The $\boldsymbol{\varphi}_{\textbf{hardening}}$ produces 76 % more signal than $\boldsymbol{\varphi}_{\textbf{standard}}$ at 500 TeV ;
- $g(r) = 1$: The $\boldsymbol{\varphi}_{\textbf{hardening}}$ produces 55% more signal than $\boldsymbol{\varphi}_{\textbf{standard}}$ at 500 TeV

After masking:

- $g(r, R = \infty)$: $\boldsymbol{\varphi}_{\textbf{hardening}}$ produces 28 % more signal than $\boldsymbol{\varphi}_{\textbf{standard}}$ at 500 TeV
- $g(r) = 1$: $\boldsymbol{\varphi}_{\textbf{hardening}}$ produces 18% more signal $\boldsymbol{\varphi}_{\textbf{standard}}$ at 500 TeV

Conclusions:

1. The total flux and the number of sources derived in *Cataldo et al 2019* based on the HGPS are compatible with the observation of KM2A within 2σ;
2. The LHAASO masks cancel most of the effect due to unresolved sources in the inner region (suppressed by 91 %). In the outer region, unresolved sources already produce a negligible contribution to the diffuse emission that is further suppressed by the LHAASO mask of about 18 %;
3. The cross-section, CR spectrum, and ISM uncertainties are non-negligible. However, the LHAASO data seems compatible with the “truly” diffuse emission within uncertainties except for the 2 low energy points in the inner region which could be explained by introducing other classes of unresolved sources.
4. The LHAASO masks significantly reduce the effect of a spatial-dependent CR spectral index. As a consequence, it is challenging to test this hypothesis using LHAASO data.

Backup slides

3. Cosmic ray distribution: $\varphi_{CR}(E,\vec{r}) = \varphi_{CR,Sun}(E)\, g(\vec{r},R)\, h(E,\vec{r})$

★ Assumption CR spectrum:

We take the data-driven CR spectrum from ***Dembinski et al 2018*** for the fiducial case and **Protons (KASKADE)** + ***Dembinski et al 2018*** to include uncertainties.

Protons

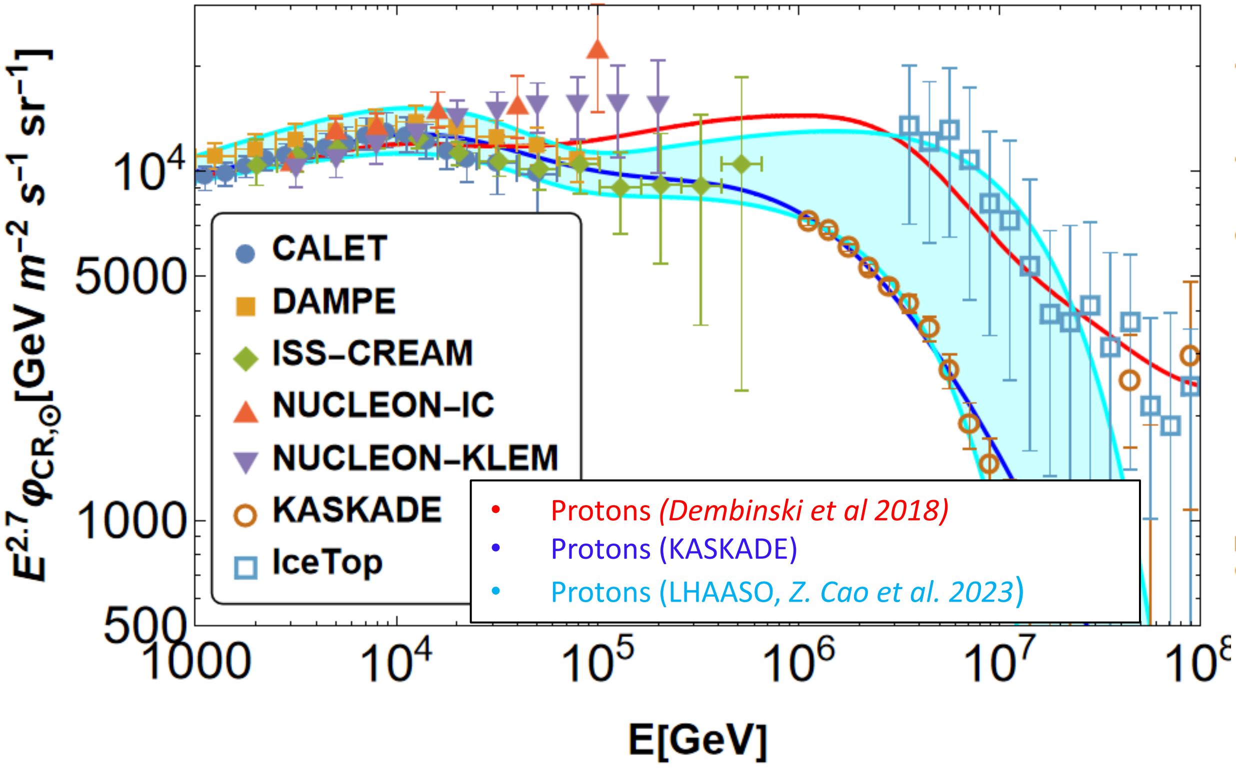

All Particle Spectrum

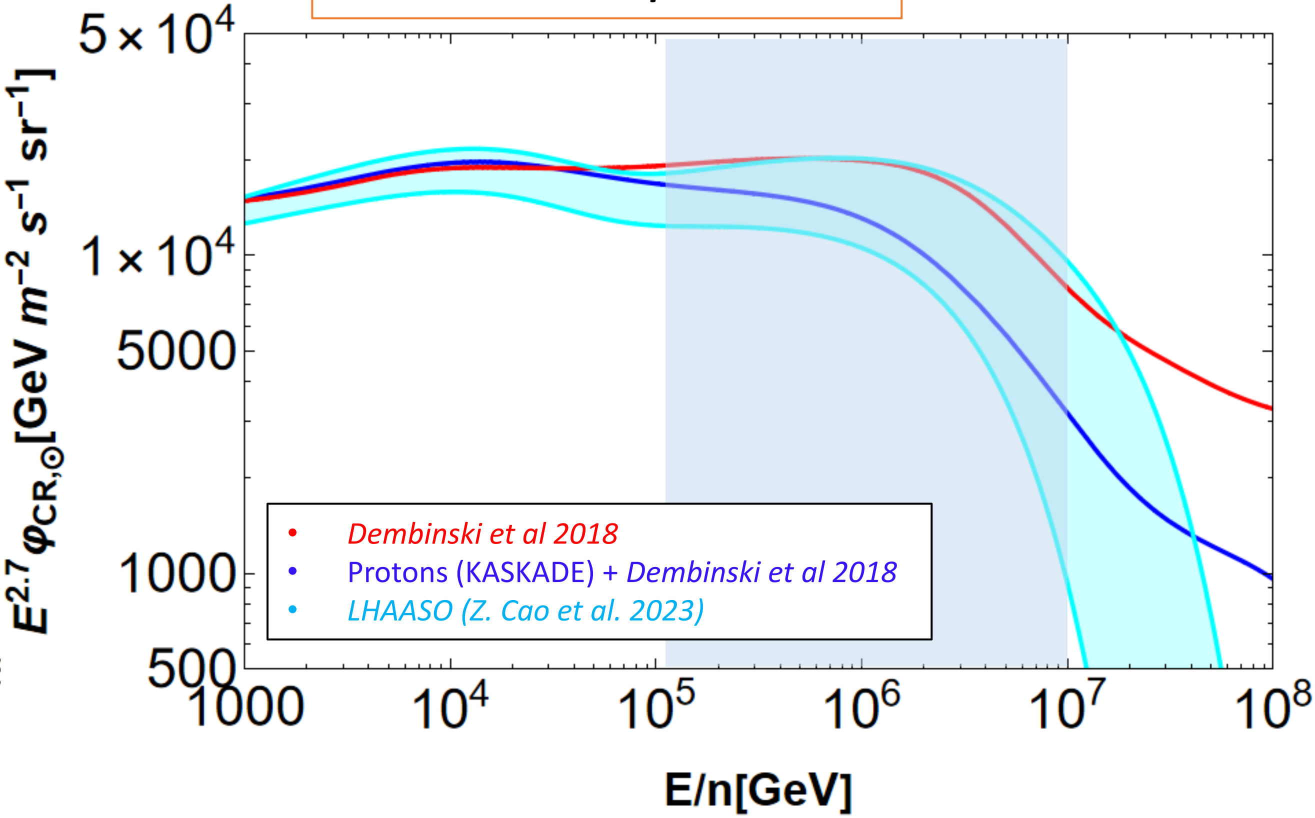

Source contributions (Size 40 pc):

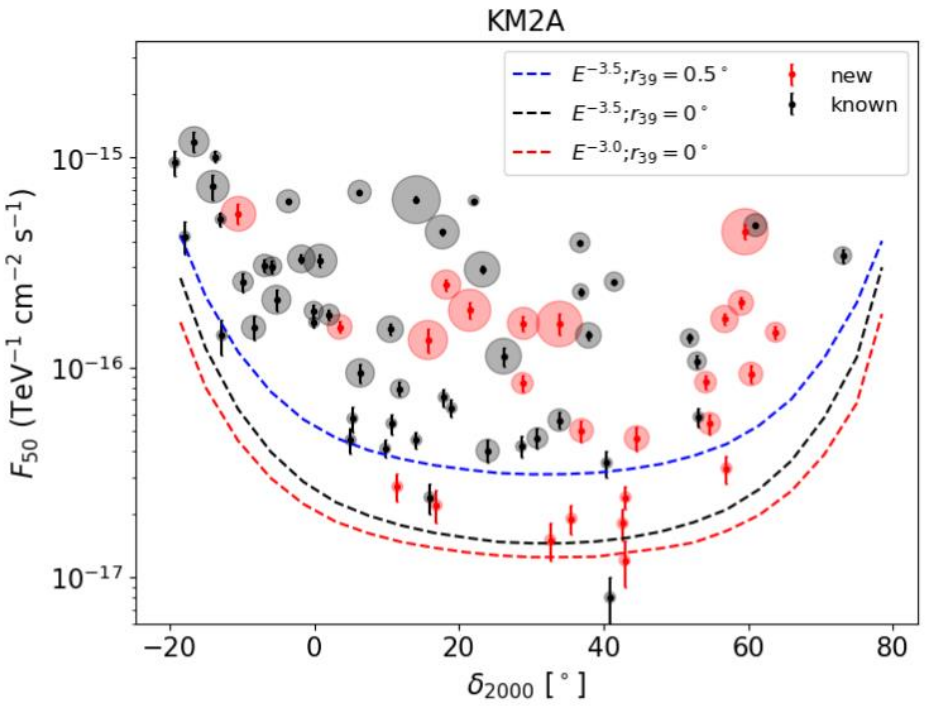

Best fit for size 40 pc:
$L_{max} = 2 \times 10^{35}$ erg/s
$\tau_{sd} = 4.6$ kyrs

Def: Resolved sources: $\phi_{50} > \phi_{th,50}\sqrt{(\sigma_{psf}^2+\sigma_s^2)/\sigma_{psf}^2}$ where $\sigma_{psf} = 0.2^\circ$ and σ_s is the angular size of the source.

		N_R	φ_R	φ_{UNR}	$\varphi_{UNR,H}$
$15^\circ < l < 235^\circ$	MC	69^{+5}_{-5}	$2.28^{+0.74}_{-0.56} \times 10^{-14}$	$7.17^{+0.37}_{-0.45} \times 10^{-15}$	–
	KM2A	76	1.72×10^{-14}	–	–
$15^\circ < l < 125^\circ$	MC	62^{+4}_{-6}	$1.76^{+0.47}_{-0.45} \times 10^{-14}$	$6.10^{+0.37}_{-0.41} \times 10^{-15}$	$8.19^{+1.74}_{-1.64} \times 10^{-16}$
	KM2A	59	1.44×10^{-14}	–	–
$125^\circ < l < 235^\circ$	MC	7^{+2}_{-1}	$4.21^{+3.4}_{-1.8} \times 10^{-15}$	$1.05^{+0.25}_{-0.27} \times 10^{-15}$	$8.32^{+2.49}_{-1.99} \times 10^{-16}$
	KM2A	16	2.75×10^{-15}	–	–

Results:

- The predicted number and flux of resolved sources are compatible with the KM2A quantities within 2σ (except in the outer region);
- The unresolved source flux is suppressed by 86 % and 20 % in the inner and outer regions, respectively.

Summary assumptions:

Assumptions for the diffuse emission fiducial model:

- CRs: *Dembinki et al 2018*;
- Gas: Galprop;
- Cross section: AAFRAG;
- CR spatial distribution of CR: $g\,(\vec{r},\infty)$

Variation with respect to the fiducial model:

- CRs: fit protons (KASKADE) + All elements (*Dembinki et al 2018*);
- Gas: Dust;
- Cross section: Sybill;
- CR spatial distribution of CR: $g\,(\vec{r},\infty)$

Assumptions unresolved sources:

- Spectrum: power-law with exponential cut-off ($\mathrm{E_{cut}} = 100$ TeV), spectral index fixed to: 2.4.
- Thickness of the disk H=0.05 kpc.

Comparison with LHAASO (hardening effect):

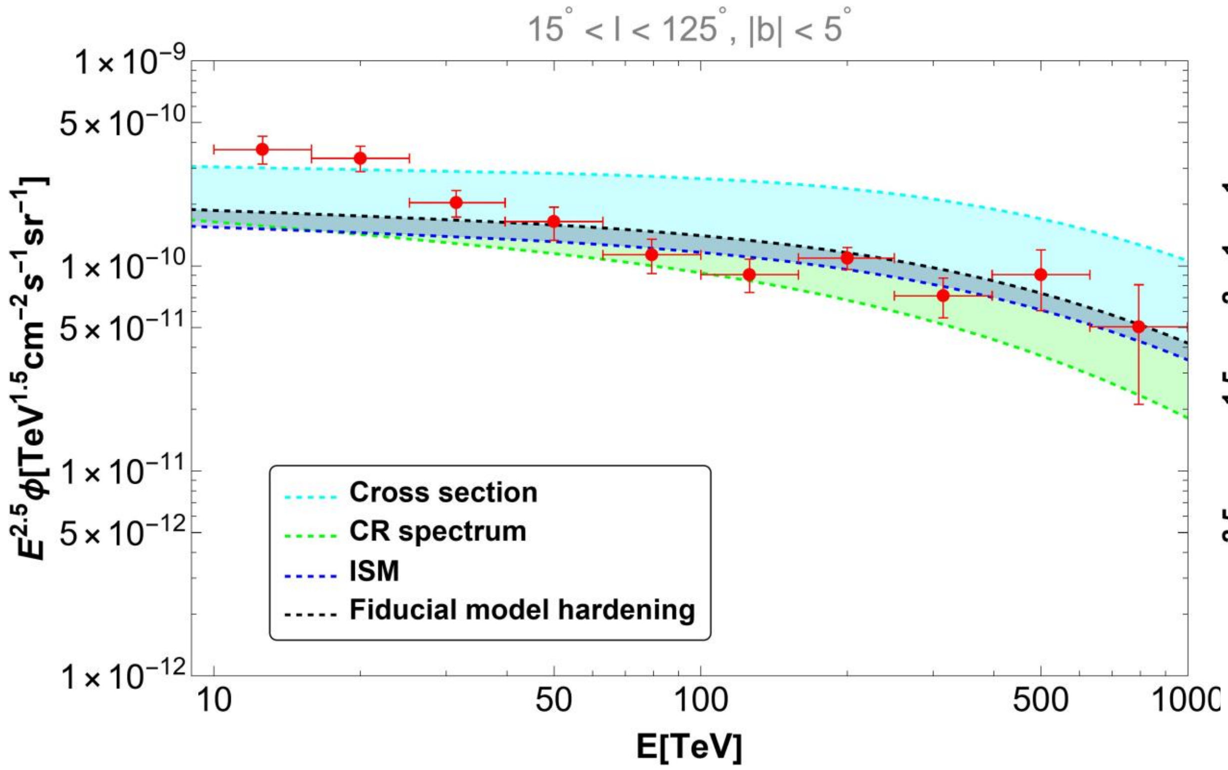

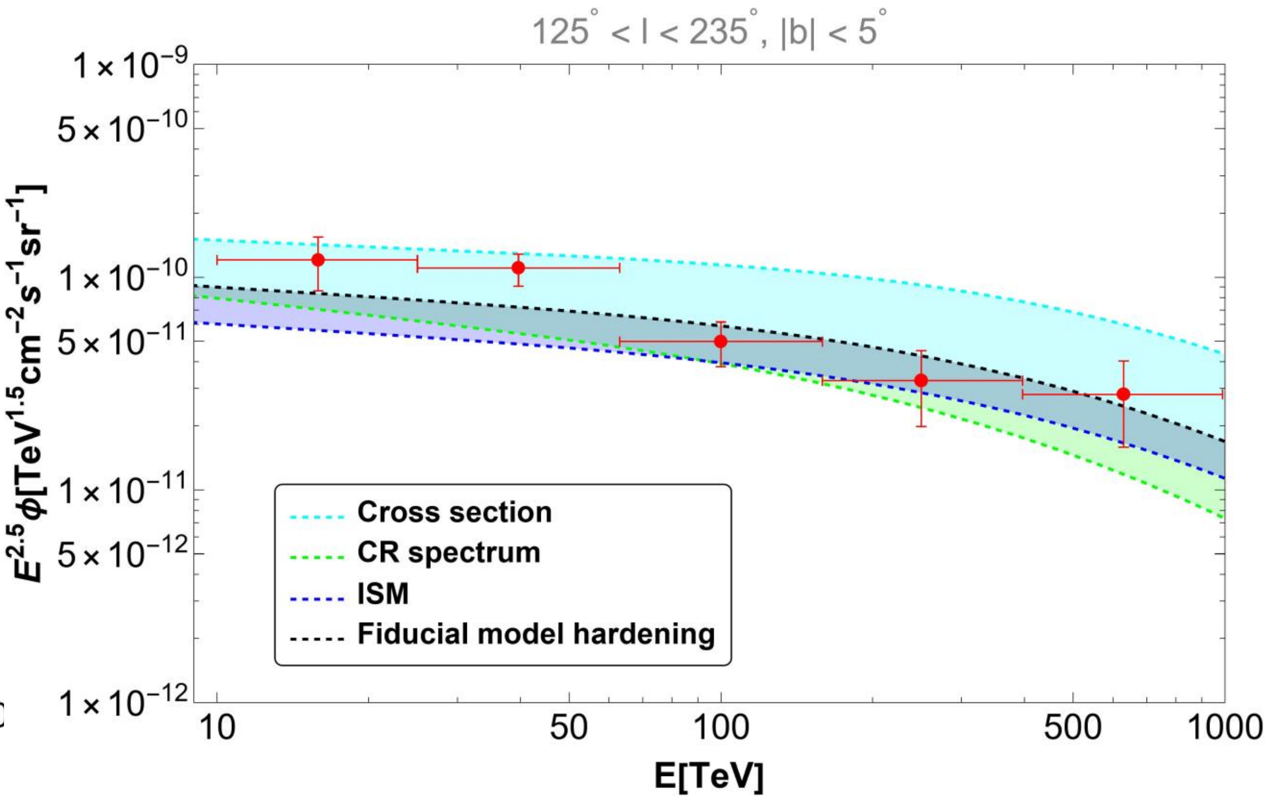

- LHAASO cannot be used to distinguish the hardening hypothesis from the standard one;

Comparison with LHAASO (standard diffusion and size 40 pc):

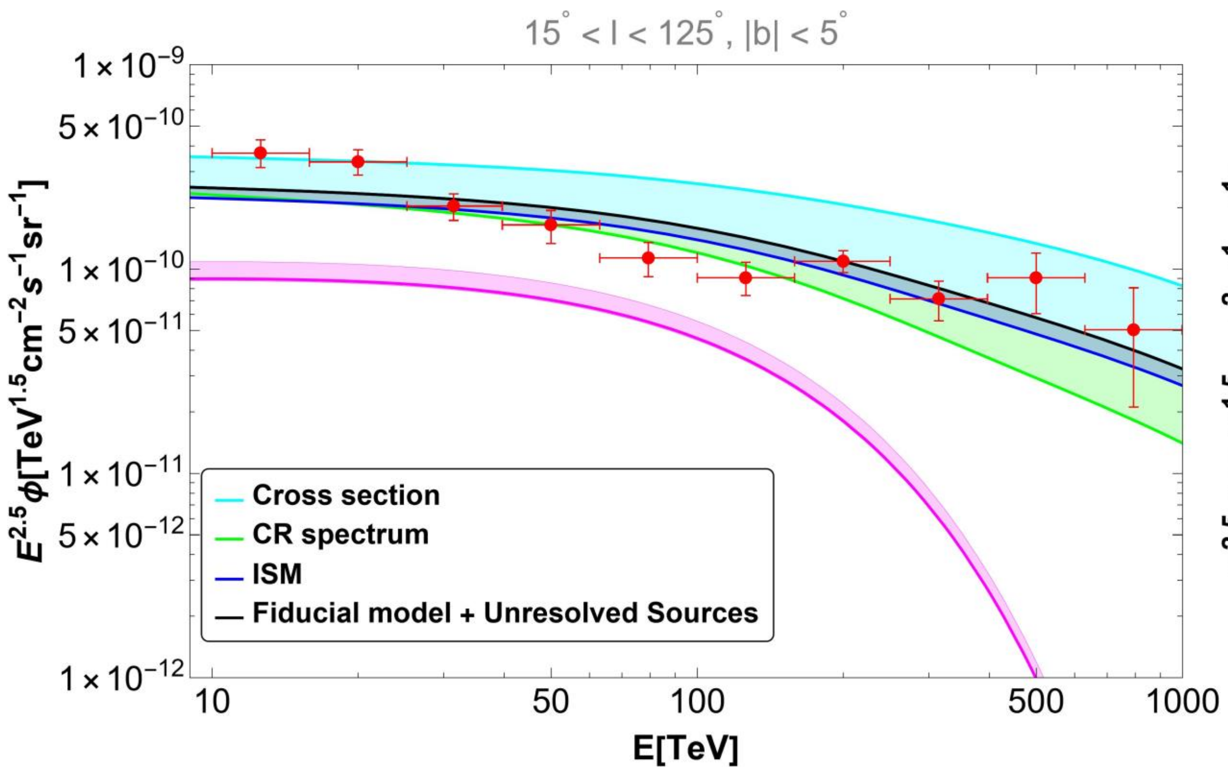

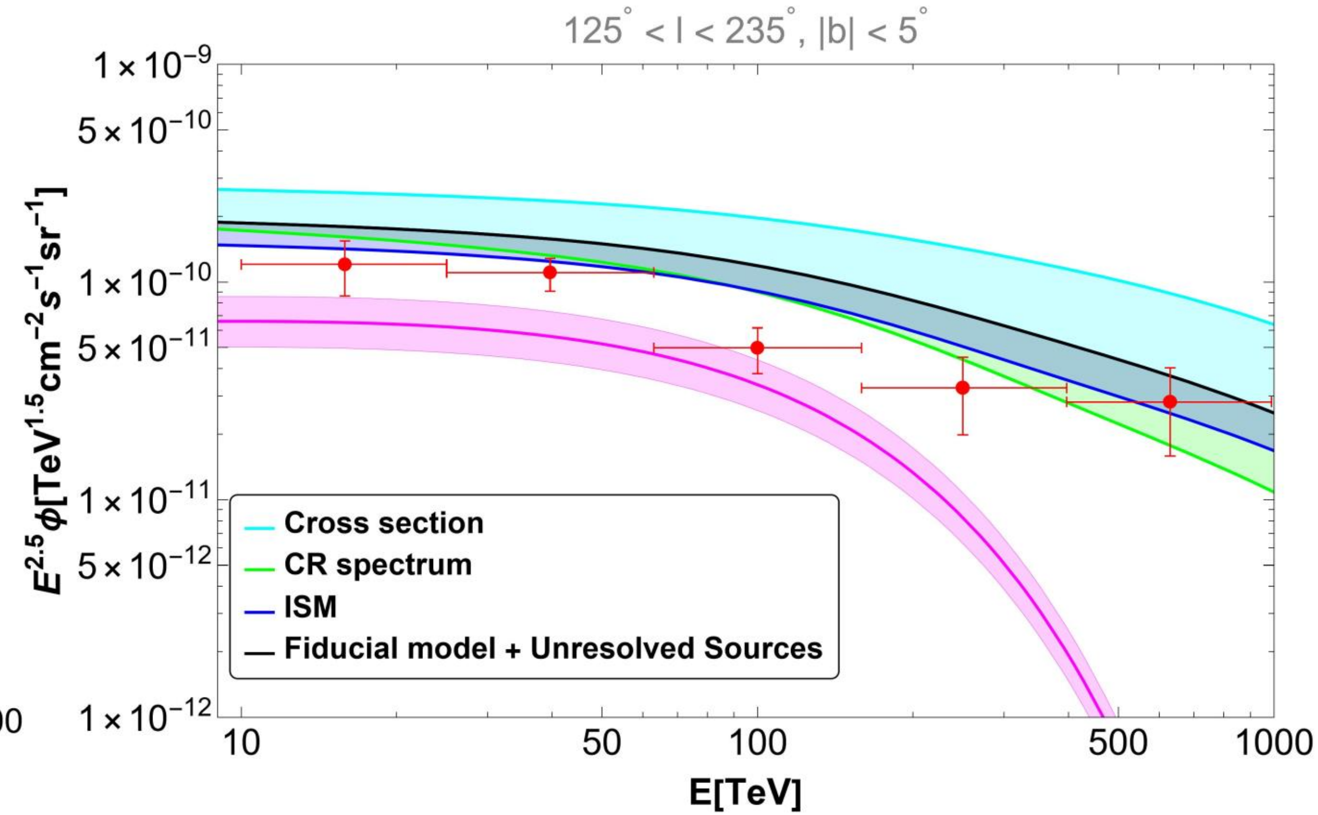

- Unresolved sources contribute $\sim 54\%$ of the fiducial model at 50 TeV in both regions;
- The 40 pc size case corresponds to an upper limit for the unresolved source contribution.